

# Probing Color Octet Electrons at the LHC

Tanumoy Mandal<sup>1,\*</sup> and Subhadip Mitra<sup>2,†</sup>

<sup>1</sup>*The Institute of Mathematical Sciences, Chennai, TN 600113, India*

<sup>2</sup>*Laboratoire de Physique Théorique, CNRS - UMR 8627,  
Univ. Paris-Sud 11, F-91405 Orsay Cedex, France*

## Abstract

Models with quark and lepton compositeness predict the existence of colored partners of the Standard Model leptons. In this paper we study the LHC phenomenology of a charged colored lepton partner, namely the color octet electron,  $e_8$ . We explore various production mechanisms of the  $e_8$ 's at the LHC. Assuming 100% branching ratio for the decay,  $e_8 \rightarrow eg$ , we estimate the LHC discovery potential for the  $e_8$ 's. Our analysis shows that the LHC with 14 TeV center of mass energy and  $100 \text{ fb}^{-1}$  ( $300 \text{ fb}^{-1}$ ) of integrated luminosity can probe  $e_8$  mass up to 3 TeV (3.4 TeV) for the compositeness scale of 5 TeV.

PACS numbers: 12.60.Rc, 14.80.-j

Keywords: Compositeness, Leptogluon, Color octet electron, LHC

---

\*Electronic address: tanumoy@imsc.res.in

†Electronic address: subhadip.mitra@th.u-psud.fr

## I. INTRODUCTION

All the experimental outcomes so far indicate that the Standard Model (SM) is the correct effective theory of elementary particles for energies below the TeV scale. The recent discovery of the Higgs boson at the Large Hadron Collider (LHC) at CERN completes the experimental verification of the particle spectrum of the SM [1, 2]. However, despite its spectacular success with the experiments, there remains some issues like the hierarchy problems, fermion family replication etc. that are not properly addressed in the SM. Many theoretical attempts have been made to resolve these issues. Among the beyond SM (BSM) alternatives, supersymmetry, extra dimensions, quark-lepton compositeness etc. are some well known examples. Many of the BSM theories predict the existence of new particles with masses near TeV scale. Two detectors of the LHC, namely the ATLAS and the CMS, are presently looking for the signatures of some of these new particles.

Of the various BSM scenarios, the quark-lepton composite models assume that the SM particles may not be fundamental and just as the proton has constituent quarks, they are actually bound states of substructural constituents (preons) [3]. These constituents are only visible beyond a certain energy scale known as the compositeness scale. A typical consequence of quark-lepton compositeness is the appearance of colored particles with nonzero lepton number (leptogluons, leptoquarks) and exited leptons etc. Some composite models naturally predict the existence of leptogluons ( $l_8$ ) [3–9] that are color octet fermions with nonzero lepton number. Several studies on the collider searches of leptoquarks, exited fermions can be found in the literature [10–12] but there are only a few similar studies on  $l_8$ 's. Various signatures of color octet leptons at different colliders were investigated in some earlier papers [13–18]. Recently some important production processes of the  $l_8$  have been analyzed for future the colliders like the Large Hadron-electron Collider (LHeC), International Linear Collider (ILC) and the Compact Linear Collider (CLiC) [19, 20]. We briefly review the limits on (charged) color octet leptons available in the literature. The lower mass limit of color octet charged leptons quoted in the latest Particle Data Book [21] is only 86 GeV. This limit is from the twenty three years old Tevatron data [22] for pair production channel. A mass limit of  $M_{l_8} > \mathcal{O}(110)$  GeV from the direct pair production via color interactions has been derived from  $p\bar{p}$  collider data in [23]. Lower limits on the leptogluons masses were derived by JADE collaboration from the  $t$ -channel contribution to the total hadronic cross section,  $M_{l_8} \gtrsim (240 \text{ GeV})^3/4\Lambda^2$  (where  $\Lambda$  is the compositeness scale) and from direct production via one photon exchange,  $M_{l_8} \gtrsim 20 \text{ GeV}$  [24]. In [25], the compositeness scale  $\Lambda \lesssim 1.8 \text{ TeV}$  was excluded at 95% CL for  $M_{l_8} \simeq 100 \text{ GeV}$  and  $\Lambda \lesssim 200 \text{ GeV}$  for  $M_{l_8} \simeq 200 \text{ GeV}$ . It is also mentioned in [17] that the D0 cross section bounds on  $eejj$  events exclude leptogluons mass up to 200 GeV and could naively place the constraint  $M_{l_8} \gtrsim 325 \text{ GeV}$ .

In this paper we study the LHC discovery potential for a generic color octet partner of charged lepton, namely the color octet electron,  $e_8$ . Although, in this paper, we consider only color octet electrons, our results are applicable for the color octet partner of muon, *i.e.*,  $\mu_8$  also. The paper is organized as follows: in Sec. II we display the interaction Lagrangian and decay width of  $e_8$ . In Sec. III we discuss various  $e_8$  production processes at the LHC. In Sec. IV we discuss the LHC reach for  $e_8$ 's. Finally, in Sec. V we summarize and offer our conclusions.

## II. THE LAGRANGIAN

Assuming lepton flavor conservation we consider a general Lagrangian for the color octet electrons including terms allowed by the gauge symmetries of the SM,

$$\mathcal{L} = \bar{e}_8^a i \gamma^\mu (\partial_\mu \delta^{ac} + g_s f^{abc} G_\mu^b) e_8^c - M_{e_8} \bar{e}_8^a e_8^a + \mathcal{L}_{int}. \quad (1)$$

For simplicity, we have ignored the terms with the electroweak couplings. The interaction part contains all the higher dimensional operators. In this paper we consider only the following dimension five terms that contain the interaction between ordinary electrons and color octet ones [21],<sup>1</sup>

$$\mathcal{L}_{int} = \frac{g_s}{2\Lambda} G_{\mu\nu}^a [\bar{e}_8^a \sigma^{\mu\nu} (\eta_L e_L + \eta_R e_R)] + H.c.. \quad (2)$$

Here  $G_{\mu\nu}^a$  is the gluon field strength tensor,  $\Lambda$  is the scale of the effective theory and  $\eta_{L/R}$  are the chirality factors. Since, electron chirality conservation implies  $\eta_L \eta_R = 0$ , we set  $\eta_L = 1$  and  $\eta_R = 0$  in our analysis.

From the interaction Lagrangian given in Eq. 2 we see that a color octet electron can decay to a gluon and an electron (two body decay mode), *i.e.*,  $e_8 \rightarrow eg$ . With  $\eta_L = 1$  and  $\eta_R = 0$ , the decay width of  $e_8$  can be written as,

$$\Gamma_{e_8} = \frac{\alpha_s (M_{e_8}) M_{e_8}^3}{4\Lambda^2}. \quad (3)$$

## III. PRODUCTION AT THE LHC

In this section we discuss various production mechanisms of  $e_8$ 's at the LHC and present the production cross sections for different channels. To obtain the cross sections, we have first implemented the Lagrangian of Eq. 1 in FeynRules version 1.6.0 [26] to generate Universal FeynRules Output (UFO) [27] format model files suitable for MadGraph5 [28] which we use to estimate the cross sections. We have used CTEQ6L1 Parton Distribution Functions (PDFs) [29] for all our numerical computations.

At a hadron collider like the LHC, the resonant production of  $e_8$ 's can occur via  $gg$ ,  $gq$  and  $qq$  initiated processes where  $q$  can be either a light quark or a bottom quark. The gluon PDF dominates at low  $x$  region whereas the quark PDFs take over at high  $x$  region. Thus, depending on its mass, all of the  $gg$ ,  $gq$  and  $qq$  initiated processes can contribute significantly to the production of  $e_8$ 's at the LHC.

For the production of on-shell  $e_8$ 's at colliders, two separate channels are generally considered in the literature – one is the pair production [17, 18] and the other is the single

---

<sup>1</sup> There are actually more dimension five operators allowed by the gauge symmetries and lepton number conservation like,

$$\frac{C_8}{\Lambda} i f^{abc} \bar{e}_8^a G_{\mu\nu}^b \sigma^{\mu\nu} e_8^c + \frac{C_1}{\Lambda} \bar{e}_8^a B_{\mu\nu} \sigma^{\mu\nu} e_8^a.$$

However these terms lead to momentum dependent  $e_8 e_8 V$  vertices (form factors). Moreover, the octet term can lead to a  $e_8 e_8 gg$  vertex which can affect the production cross section. We assume the unknown coefficients associated with these terms are negligible.

production of an  $e_8$  [13–16, 19]. In general, pair production of a colored particle is considered mostly model independent. This is because the universal strong coupling constant  $g_s$  controls the dominant pair production processes unlike the single production processes where the cross section depends more on various model parameters like couplings and scales etc. However, as we shall see, for  $e_8$ 's, the  $t$ -channel electron exchange diagrams can contribute significantly to the pair production making it more model dependent.

### A. Pair Production ( $gg, qq \rightarrow e_8 e_8$ )

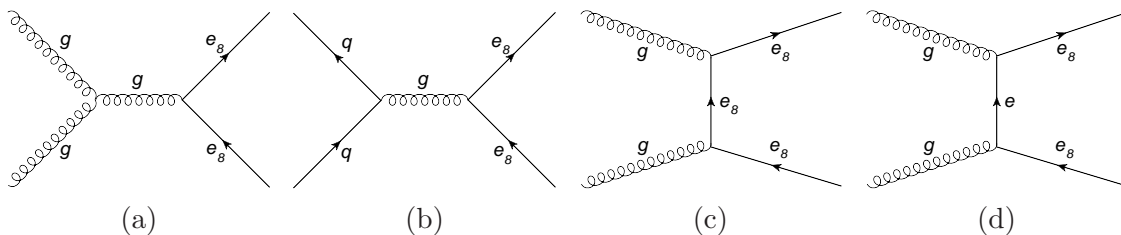


FIG. 1: Parton level Feynman diagrams for  $pp \rightarrow e_8 e_8$  process at the LHC.

The pair production of  $e_8$ 's can proceed through the  $gg$  and  $qq$  initial states - see Fig. 1 where we have shown some sample parton level Feynman diagrams for the pair production of  $e_8$  at the LHC. Of these, only the electron exchange diagram, shown in Fig. 1d, contains the  $\Lambda$  dependent  $gee_8$  vertex. In Fig. 2 we show the  $pp \rightarrow e_8 e_8$  cross sections as a function of  $M_{e_8}$  for two different choices of  $\Lambda$ ,  $\Lambda = M_{e_8}$  and  $\Lambda = 5$  TeV, at the 14 TeV LHC. In Fig. 3 we have plotted  $\delta\sigma$  as a function of  $\Lambda$  to show the dependence of the pair production cross section on  $\Lambda$  for  $M_{e_8} = 1$  and 2 TeV, where  $\delta\sigma$  is defined as,

$$\delta\sigma(\Lambda) = \sigma(\Lambda) - \sigma(\Lambda \rightarrow \infty). \quad (4)$$

As  $\Lambda$  increases the contribution coming from the electron exchange diagrams decreases and for  $\Lambda \gg M_{e_8}$  becomes negligible. So the pair production is model independent only for very large  $\Lambda$ . Moreover this  $\Lambda$  dependence becomes more prominent for smaller  $M_{e_8}$ .

After being produced as pairs at the LHC, each  $e_8$  decays into an electron (or a positron) and a gluon at the parton level, i.e.,  $e_8 e_8 \rightarrow eejj$ . For large  $M_{e_8}$ , these two jets and the lepton pair will have high  $p_T$ . This feature can be used to isolate the  $e_8$  pair production events from the SM backgrounds at the LHC.

### B. Two body Single Production ( $gg, qq \rightarrow e_8 e$ )

The two body single production channel where an  $e_8$  is produced in association with an electron can proceed through the  $gg$  and  $qq$  initial states as shown in Fig. 4. This channel is model dependent as each Feynman diagram for  $pp \rightarrow e_8 e$  process always contains  $\Lambda$  dependent vertex. In Fig. 5 we show the  $pp \rightarrow e_8 e$  cross sections as a function of  $M_{e_8}$  with  $\Lambda = M_{e_8}$  and 5 TeV at the 14 TeV LHC.

As the  $e_8$  decays this process gives rise to a  $eej$  final state at the parton level. The  $e$  and the  $j$  produced from the decay of the  $e_8$ , have high  $p_T$ . The other  $e$  also possesses very high  $p_T$  as it balances against the massive  $e_8$ .

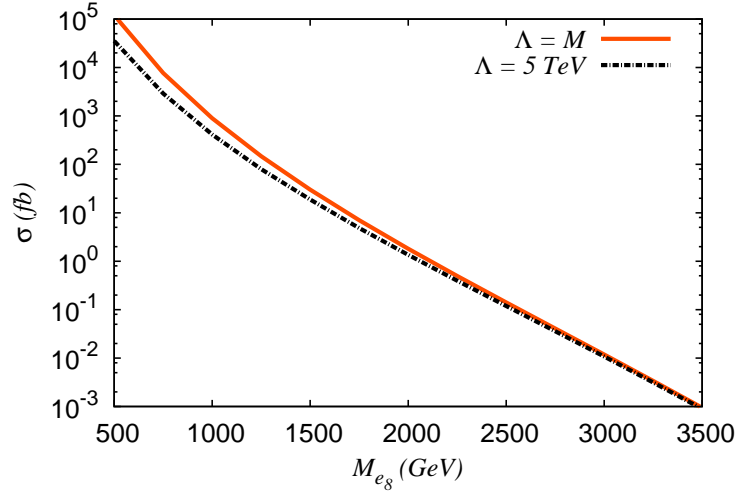


FIG. 2: The cross sections for  $pp \rightarrow e_8 e_8$  as a function of  $M_{e_8}$  for  $\Lambda = M_{e_8}$  and  $\Lambda = 5$  TeV at the 14 TeV LHC.

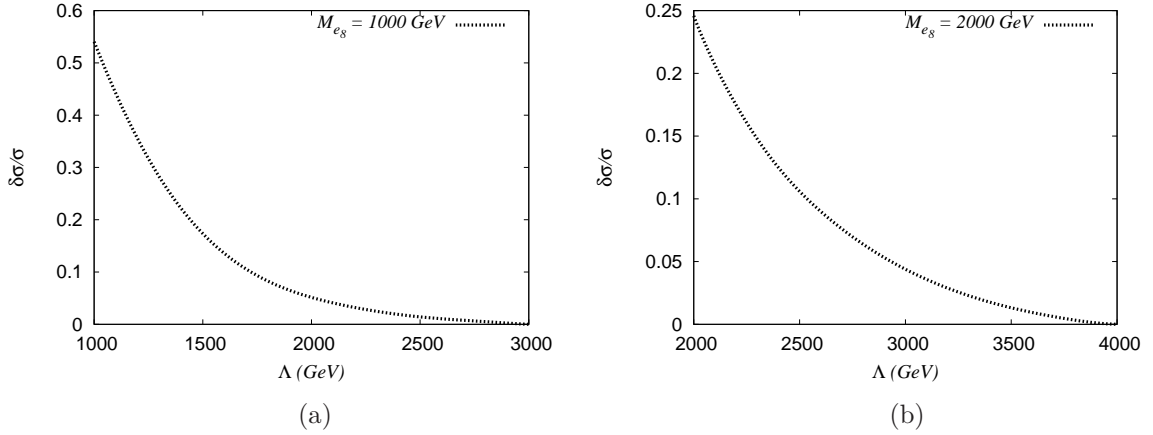


FIG. 3: Dependence of  $\delta\sigma/\sigma$  (defined in Eq. 4) on  $\Lambda$  for (a)  $M_{e_8} = 1$  TeV and (b)  $M_{e_8} = 2$  TeV at the 14 TeV LHC.

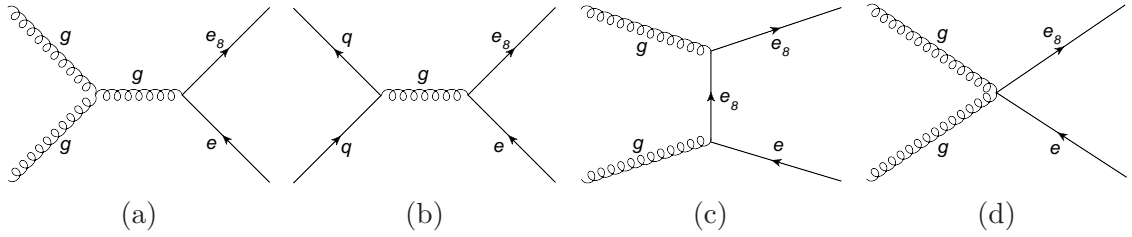


FIG. 4: Parton level Feynman diagrams for  $pp \rightarrow e_8 e$  process at the LHC.

### C. Three body Single Production ( $gg, gq, qq \rightarrow e_8 e j$ )

Apart from the pair and two body single productions, we also consider the single production of an  $e_8$  in association with an electron and a jet. The  $pp \rightarrow e_8 e j$  process

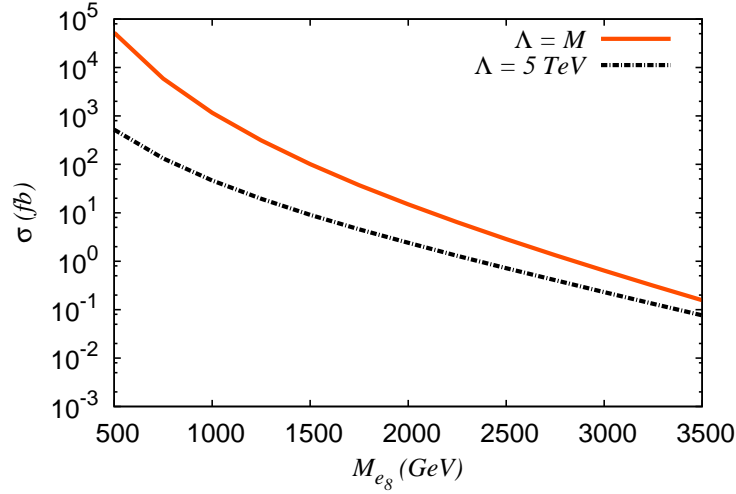


FIG. 5: The cross sections for  $pp \rightarrow e_8 e$  as a function of  $M_{e_8}$  for  $\Lambda = M_{e_8}$  and  $\Lambda = 5 \text{ TeV}$  at the 14 TeV LHC.

includes three different types of diagrams as follows.

1. The pair production of  $e_8$ 's with only one  $e_8$  decaying into an  $e j$  pair can give rise to an  $e_8 e j$  final state. Though there are three particles in the final state, these type of diagrams effectively correspond to two body processes.
2. The two body single production ( $pp \rightarrow e_8 e$ ) process with a jet radiated from initial state (ISR) or final state (FSR) or intermediate virtual particles can lead to an  $e_8 e j$  final state.
3. A new set of diagrams that are different from the two types of diagrams mentioned above. These new channels can proceed through  $g g$ ,  $q q$  and  $g q$  initial states as shown in Fig. 6.

This new set of diagrams has not been considered so far in the literature. However, it is difficult to compute the total contribution of these diagrams in a straight forward manner with a leading order parton level matrix element calculation because of the presence of soft radiation jet emission diagrams. In order to get an estimation of the contribution of these new diagrams without getting into the complicity of evaluating the soft jet emission diagrams, here, in this section, we present the cross section only for the  $g q$  initiated processes, i.e.  $g q \rightarrow e_8 e j$  since the first and the second types of diagrams can not be initiated by  $g q$  state. In Fig. 8 we show the cross section of the  $g q \rightarrow e_8 e j$  process along with  $pp \rightarrow e_8 e_8$  and  $pp \rightarrow e_8 e$  processes. We find that the cross section even for the  $g q$  initiated subset are comparable to the  $pp \rightarrow e_8 e$  process for large  $M_{e_8}$  despite the facts that these new diagrams have three body final states and are suppressed by one extra power of the coupling compared to the two body single and pair production processes. However, since there is one extra heavy  $e_8$  in the pair production process, the three body phase space of the single production can be comparable or even larger to the two body phase space of the pair production for large  $M_{e_8}$ .

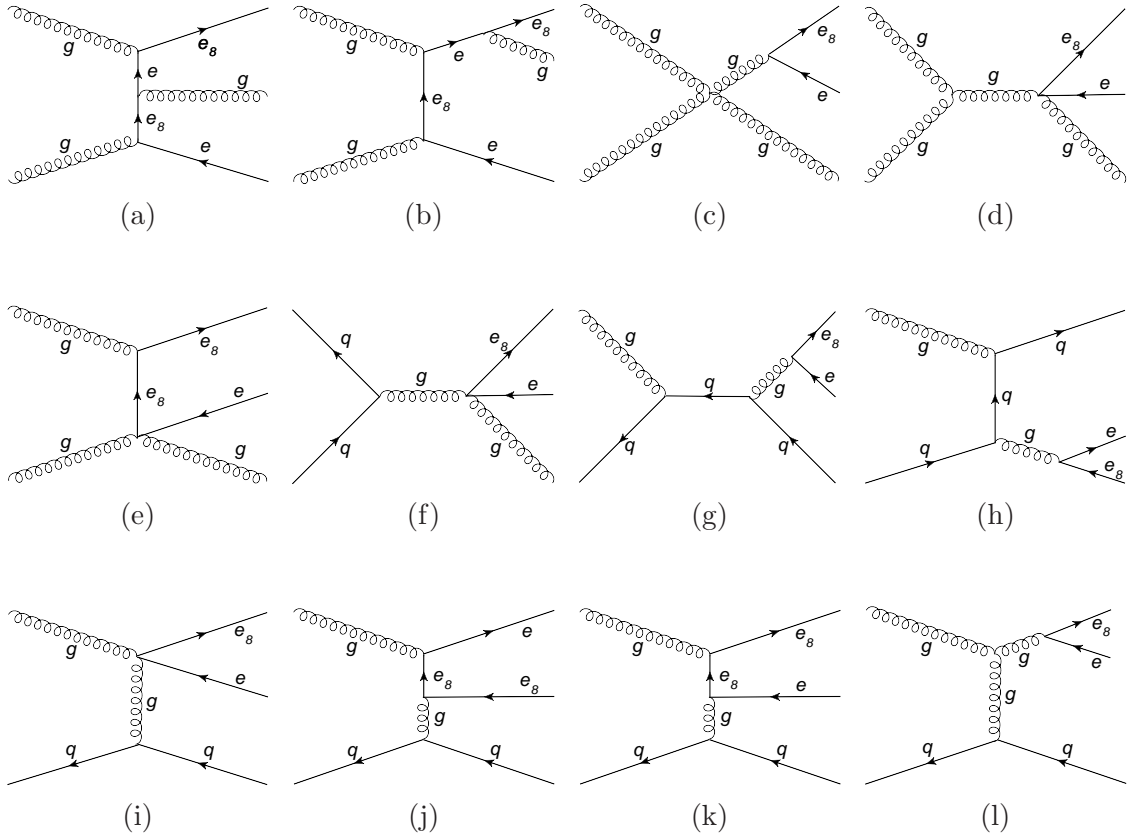


FIG. 6: Parton level Feynman diagrams for  $pp \rightarrow e_8 e j$  process of third type at the LHC.

After the  $e_8$  decay the three body single production process is characterized by an  $eejj$  final state like the pair production. However unlike the pair production, here one of the jet can have a low transverse momentum.

#### D. Indirect Production ( $gg \rightarrow ee$ )

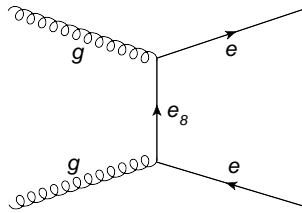


FIG. 7: Parton level Feynman diagram for indirect production of  $e_8$ 's at the LHC.

So far we have considered only resonant production of  $e_8$ 's. However, a t-channel exchange of the  $e_8$  can convert a gluon pair to an electron-positron pair at the LHC (Fig. 7). Similar indirect productions in the context of the future linear colliders such as the ILC and CLIC have been analyzed in [20]. Indirect production is less significant because the amplitude is proportional to  $1/\Lambda^2$ . Moreover, at the LHC this is also color suppressed

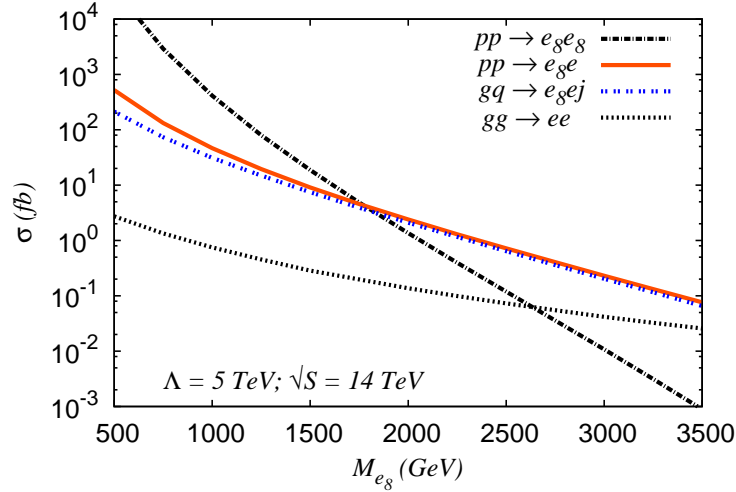


FIG. 8: Cross sections for  $pp \rightarrow e_8 e_8$ ,  $pp \rightarrow e_8 e$ ,  $gq \rightarrow e_8 e j$  and  $gg \xrightarrow{e_8} ee$  processes for  $\Lambda = 5$  TeV at the 14 TeV LHC. The  $\sigma(gq \rightarrow e_8 e j)$  is computed with the following kinematical cuts:  $p_T(j) > 25$  GeV and  $|y(j)| < 2.5$ .

because of the color singlet nature of the final states. In Fig. 8 we also show the cross section of the indirect production process at the LHC

#### IV. LHC DISCOVERY POTENTIAL

From Fig. 8 we see that for small  $M_{e_8}$  the pair production cross section is larger than the other channels. However, as  $M_{e_8}$  increases it decreases rapidly due to phase-space suppression and the single production channels (both the two body and three body) take over the pair production (the cross over point depends on  $\Lambda$ ). So, a search with a signal selection criterion that combines the events from both pair and single production channels is expected to perform better than one that uses the individual production channels if  $\Lambda$  is not too high. Moreover, because of the radiation jets, it will be very difficult to separate the two body and the three body single production at the LHC. In this paper, we shall construct a selection criterion that combines all the production processes at the LHC.

##### Combined Signal

To design such a selection criterion we first note some of the characteristics of the final states of the on-shell production processes,<sup>2</sup>

1. Process  $pp \rightarrow e_8 e_8 \rightarrow (eg)(eg)$  has two high  $p_T$  electrons and two high  $p_T$  jets in the final state.

<sup>2</sup> We focus on the on-shell production because as we saw the indirect production is less significant at the LHC.



2. Process  $pp \rightarrow e_8 e \rightarrow (eg)e$  has two high  $p_T$  electrons and one high  $p_T$  jet in the final state.
3. Process  $pp \rightarrow e_8 ej \rightarrow (eg)ej$  has two high  $p_T$  electrons and at least one high  $p_T$  jet in the final state.

All these processes have one common feature that they have two high  $p_T$  electrons and a high  $p_T$  jet in the final state. Hence if we demand that the signal events should have two high  $p_T$  electrons and at least one high  $p_T$  jet, we can capture events from all the above mentioned production processes. However, as already pointed out, it is difficult to estimate the number of signal events that passes the above selection criterion with only a matrix element (ME) level Monte Carlo computation due to the presence of soft radiation jets. Hence we use the MadGraph ME generator to compute the hard part of the amplitude and Pythia6 (via the MadGraph5-Pythia6 interface) for parton showering. We also match the the matrix element partons with the parton showers to estimate the inclusive signal without double counting the contribution of some diagrams (see the Appendix A for more details on the matched signal).

## Backgrounds

With the selection criterion mentioned above, the SM backgrounds are characterized by the presence of two opposite sign electrons and at least one jet in the final state. At the LHC, the main source of  $e^+e^-$  pairs (with high  $p_T$ ) is the  $Z$  decay<sup>3</sup>. Hence we compute the inclusive  $Z$  production as the main background. Here, too, we compute this by matching of matrix element partons of  $Z + n$  jets ( $n = 0, 1, 2, 3$ ) processes<sup>4</sup> with the parton showers using the shower- $k_T$  scheme [30]. For the background, we also consider some potentially significant processes to produce  $e^+e^-$  pairs,

$$\begin{aligned} pp &\rightarrow tt \rightarrow (bW)(bW) \rightarrow (be\nu_e)(be\nu_e), \\ pp &\rightarrow tW \rightarrow bWW \rightarrow (be\nu_e)(e\nu_e), \\ pp &\rightarrow WW \rightarrow (e\nu_e)(e\nu_e). \end{aligned}$$

Note that all these processes have missing energy because of the  $\nu_e$ 's in the final state. In Table I we show the relative contributions of these backgrounds generated with some basic kinematical cuts on the final states to be described shortly. As mentioned, the inclusive  $Z$  production overwhelms the other processes.

## Kinematical Cuts

In Fig. 9a we display the  $p_T$  distributions of  $e^-$ 's from the combined signal and the inclusive  $Z$  production, respectively. For the signal, we have chosen  $M_{e_8} = 2$  TeV and

<sup>3</sup> The  $e^+e^-$  pairs can come from  $\gamma^*$  also which we don't consider here. However, as we shall demand very high  $p_T$  for both the electrons, this background becomes negligible and won't affect our results too much.

<sup>4</sup> Here  $pp \rightarrow Zjj$  includes the processes where the jets are coming from a  $W, Z$ .

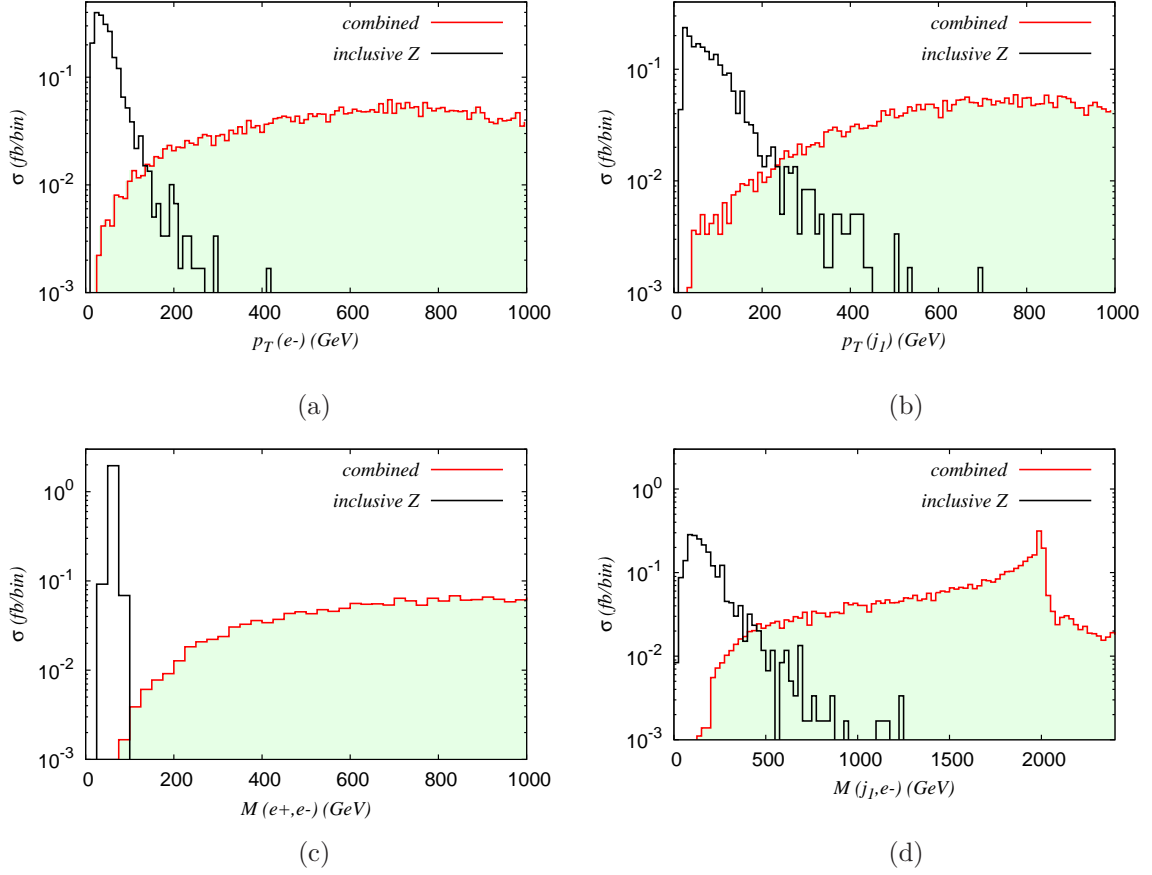


FIG. 9: Comparison between various distributions for the combined signal with  $M_{e_8} = 2$  TeV ( $\Lambda = 5$  TeV) and the inclusive  $Z$  background for the 14 TeV LHC. The inclusive  $Z$  background is scaled by a factor of  $10^4$ .

Process	Cross section (fb)
$Z + nj$	$2.11E4$
$tt$	$1.95E3$
$tW$	132.15
$WW$	7.51
Total	$2.32E4$

TABLE I: The main SM backgrounds to the combined production of  $e_8$ 's obtained after applying the Basic cuts (see text for definition).

$\Lambda = 5$  TeV. As expected, the distribution for the  $e^-$  coming from the background has a peak about  $M_Z/2$  but there is no such peak for the signal. We can also see the difference between the  $p_T$  distributions of the leading  $p_T$  jets for the signal and the background in Fig. 9b. In the same figure we have also plotted the distributions of  $M(e^+, e^-)$  (see Fig.9c) and  $M(e^-, j_1)$  (see Fig. 9d) (where  $j_1$  denotes the leading  $p_T$  jet) which show very different nature for the signal and the background.

Motivated by these distributions we construct some kinematical cuts to separate the

$M$ (GeV)	Basic (fb)	Cut-I (fb)	Cut-II (fb)
500	2.74E4	7.51E3	1.81E4
1000	443.63	344.90	343.45
1500	31.76	28.22	22.74
2000	4.77	4.34	2.98
2500	1.18	1.07	0.64
3000	0.37	0.34	0.18
3500	0.13	0.12	0.06

TABLE II: The combined signal with three different kinematical cuts (see text for the definitions of the cuts) for different  $M_{e_8}$ .

signal from the background.

### 1. Basic cuts

For  $x, y = e^+, e^-, j_1, j_2$  ( $j_1$  and  $j_2$  denote the first two of the  $p_T$  ordered jets respectively),

- (a)  $p_T(x) > 25$  GeV
- (b) Rapidity,  $|y(x)| < 2.5$
- (c) Radial distance,  $\Delta R(x, y)_{x \neq y} \geq 0.4$

### 2. Cut-I

- (a) All the *Basic* cuts
- (b)  $p_T(e^+/e^-) > 200$  GeV;  $p_T(j_1) > 100$  GeV
- (c)  $M(e^+, e^-) > 150$  GeV

### 3. Cut-II

- (a) All the *Basic* cuts
- (b)  $p_T(e^+/e^-) > 150$  GeV;  $p_T(j_1) > 100$  GeV
- (c)  $|M(e, j_i) - M_{e_8}| \leq 100$  GeV where  $e = e^+$  or  $e^-$  and  $j_i = j_1$  or  $j_2$ .

In Cut-I and Cut-II we consider two different invariant mass cuts. The invariant mass cut on  $M(e^+, e^-)$  is used in Cut-I to reduce the  $Z$  inclusive background. This cut reduces the total background shown in Table I to about 1.7 fb. In Cut-II, we demand that either of the electrons reconstruct an  $e_8$  when combined with any one of  $j_1$  or  $j_2$  which can also increase the signal to background ratio. However, unlike Cut-I, Cut-II depends on an unknown parameter, namely,  $M_8$  and so implementing this requires scanning over a range of  $M_{e_8}$ . We find that this cut can reduce the SM background drastically. Especially for higher  $M_{e_8}$  the background becomes much smaller compared to the signal, making it essentially background free. In Table II we show the signal with the three different cuts applied.

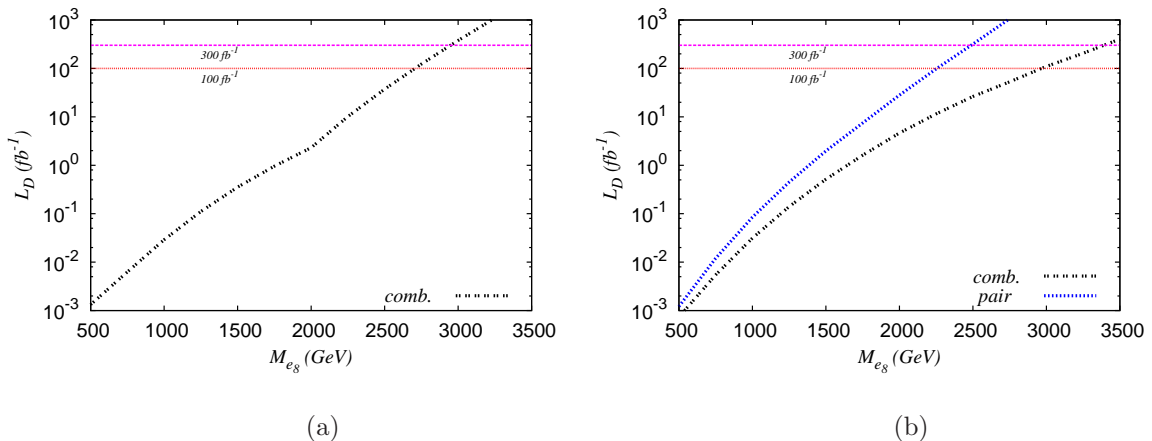


FIG. 10: The required luminosity for discovery ( $L_D$ ) as a function of  $M_{e_8}$  with  $\Lambda = 5$  TeV at the 14 TeV LHC for combined production with (a) Cut-I and (b) Cut-II (see text for the definitions of the cuts). In (b), the  $L_D$  for pair production is computed after demanding two  $e_8$ 's are reconstructed instead of one defined in Cut-II.

### LHC Reach with Combined Signal

We define the luminosity requirement for the discovery of color octet electrons at the LHC as following:

$$L_D = \text{Max}(L_5, L_{10}) \quad (5)$$

where  $\mathcal{L}_5$  denotes the luminosity required to attain  $5\sigma$  statistical significance for  $S/\sqrt{B}$  and  $\mathcal{L}_{10}$  is the luminosity required to observe 10 signal events. We show  $L_D$  as a function of  $M_{e_8}$  for Cut-I (Cut-II) in Fig. 10a (10b) for  $\Lambda = 5$  TeV. In Fig. 10b we also plot the  $L_D$  using only the pair production process. For the pair production we apply a kinematical cut almost identical to Cut-II except that now we demand that the two electrons and the two leading  $p_T$  jets reconstruct to two  $e_8$ 's instead of one. The small dip near 2 TeV in Fig. 10a appears due the transition of  $L_D$  from  $L_{10}$  to  $L_5$ . We see that even with such a simple cut the LHC can probe color octet electrons with mass about 2.7 TeV (2.9 TeV) with  $100 \text{ fb}^{-1}$  ( $300 \text{ fb}^{-1}$ ) luminosity. In Fig. 10b,  $L_D$  goes as  $L_{10}$  for both pair and combined productions, as in these cases the backgrounds become quite small (almost negligible for large  $M_{e_8}$ ) compared to the signals. With Cut-II the reach goes up to 3 TeV (3.4 TeV) with  $100 \text{ fb}^{-1}$  ( $300 \text{ fb}^{-1}$ ) luminosity. This also shows that for  $\Lambda = 5$  TeV with combined signal the reach goes up from the pair production by almost 0.9 TeV. However we should keep in mind that this increase depends on  $\Lambda$ . As the single production cross section goes like  $1/\Lambda^2$ , if  $\Lambda$  is smaller than 5 TeV then the reach of the combined production will increase even more but for higher  $\Lambda$  its  $L_D$  plot will approach more towards the pair production plot.

## V. SUMMARY AND CONCLUSIONS

In this paper we have studied the phenomenology of  $e_8$ 's at the LHC and estimated the discovery potential of the LHC for such particles. We have explored various production

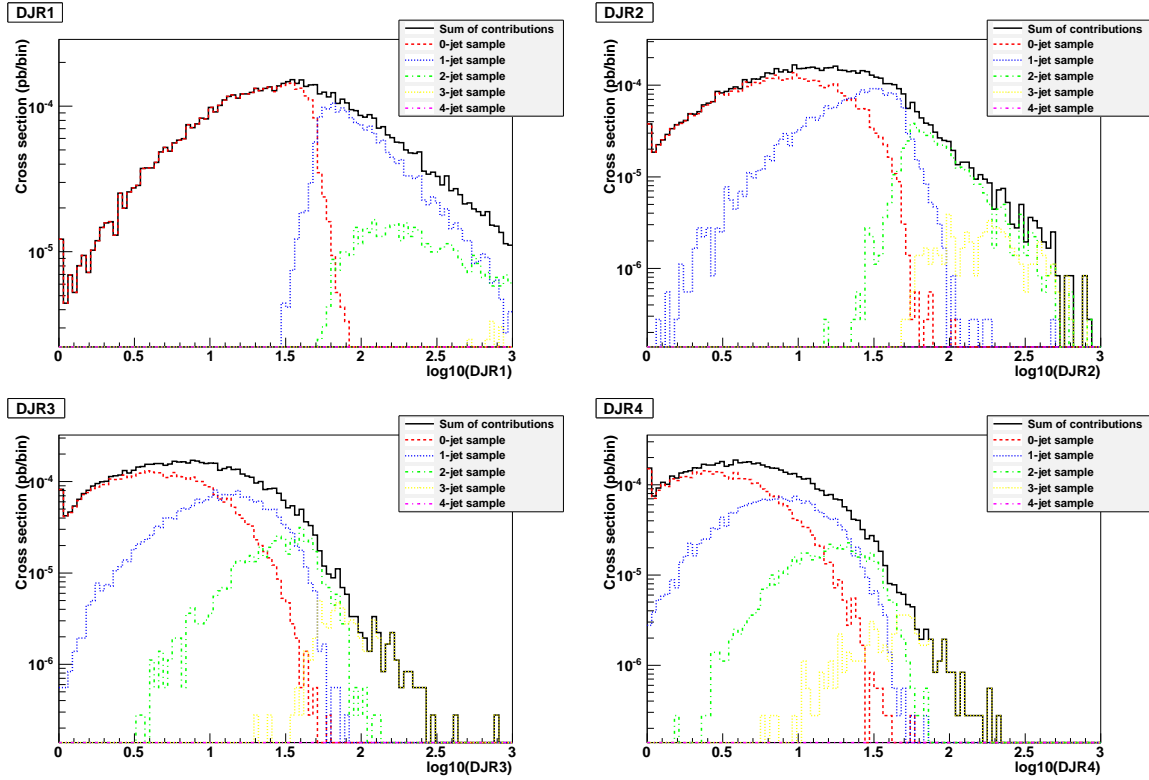


FIG. 11: Differential jet rate (DJR) plots for the signal for  $M_{e_8} = 2$  TeV with  $\Lambda = 5$  TeV at the 14 TeV LHC.

channels of  $e_8$ 's at the LHC namely, the pair, the two body single, the three body single and the indirect production channels. We have considered a new set of three body single production diagrams whose contribution can be comparable to other channels. While the pair production cross section dominates the other channels for low  $M_{e_8}$ , for high values of  $M_{e_8}$  the single productions become significant. The 14 TeV LHC with  $300 \text{ fb}^{-1}$  integrated luminosity can probe  $e_8$ 's with mass up to 2.4 TeV with only pair production. We have demonstrated how this reach can be increased further by combining signal events from different production processes. However, this increment is  $\Lambda$  dependent as the single production cross sections scales as  $1/\Lambda^2$ . For  $\Lambda = 5$  TeV the increment is about a TeV.

Finally we note that the data from the current leptoquark searches at the LHC can be used to search for  $e_8$ 's also. It is possible that the current data [10, 11] already puts some strong constraints on the mass of the  $e_8$ 's. We postpone the analysis of the recent LHC data to put limits on  $e_8$  parameters for future research.

### Acknowledgements

We thank J. Alwall and F. Maltoni for helping us with matching. SM thanks R. Barcelo for helpful comments.

## Appendix A: Preparation of Matched Signal

For the signal, we match the matrix element partons with the parton showers using the shower- $k_T$  scheme [30] in MadGraph5 with the matching scale  $Q_{cut} \sim 50$ . We generate the combined signal including the different production processes as discussed in section IV,

$$\begin{aligned}
pp &\xrightarrow{e_8} ee \text{ (includes } P_{ind}) \\
pp &\xrightarrow{e_8} ee + 1\text{-j (includes } P_{ind} + 1\text{-j, } P_{2Bs}) \\
pp &\xrightarrow{e_8} ee + 2\text{-j (includes } P_{ind} + 2\text{-j, } P_{2Bs} + 1\text{-j, } P_{pair}, P_{3Bs}^3) \\
pp &\xrightarrow{e_8} ee + 3\text{-j (includes } P_{ind} + 3\text{-j, } P_{2Bs} + 2\text{-j, } P_{pair} + 1\text{-j, } P_{3Bs}^3 + 1\text{-j)} \quad (A1)
\end{aligned}$$

where  $P_{pair}$ ,  $P_{2Bs}$ ,  $P_{3Bs}^3$  and  $P_{ind}$  are the pair, two body single, three body single of 3rd type and indirect productions respectively. In Fig. 11 we show the differential jet rate (DJR) plots obtained for a typical value of  $M_{e_8} = 2$  TeV. We refer the reader to [30] and the references therein for more details on the matching scheme and the procedure.

- 
- [1] G. Aad *et al.* [ATLAS Collaboration], Phys. Lett. B **716**, 1 (2012) [arXiv:1207.7214 [hep-ex]].
  - [2] S. Chatrchyan *et al.* [CMS Collaboration], Phys. Lett. B **716**, 30 (2012) [arXiv:1207.7235 [hep-ex]].
  - [3] J. C. Pati and A. Salam, Phys. Rev. D **10**, 275 (1974) [Erratum-ibid. D **11**, 703 (1975)].
  - [4] H. Terazawa, K. Akama and Y. Chikashige, Phys. Rev. D **15**, 480 (1977).
  - [5] Y. Ne'eman, Phys. Lett. B **81**, 190 (1979).
  - [6] H. Harari, Phys. Lett. B **86**, 83 (1979).
  - [7] M. A. Shupe, Phys. Lett. B **86**, 87 (1979).
  - [8] H. Fritzsch and G. Mandelbaum, Phys. Lett. B **102**, 319 (1981).
  - [9] I. A. D'Souza and C. S. Kalman, Singapore, Singapore: World Scientific (1992) 108 p
  - [10] S. Chatrchyan *et al.* [CMS Collaboration], Phys. Rev. D **86**, 052013 (2012) [arXiv:1207.5406 [hep-ex]].
  - [11] S. Chatrchyan *et al.* [CMS Collaboration], arXiv:1210.5629 [hep-ex].
  - [12] G. Aad *et al.* [ATLAS Collaboration], Phys. Rev. D **85**, 072003 (2012) [arXiv:1201.3293 [hep-ex]].
  - [13] T. G. Rizzo, Phys. Rev. D **33**, 1852 (1986).
  - [14] T. G. Rizzo, Phys. Rev. D **34**, 133 (1986).
  - [15] K. H. Streng, Z. Phys. C **33**, 247 (1986).
  - [16] A. Celikel and M. Kantar, Turk. J. Phys. **22**, 401 (1998).
  - [17] J. L. Hewett and T. G. Rizzo, Phys. Rev. D **56**, 5709 (1997) [hep-ph/9703337].
  - [18] A. Celikel, M. Kantar and S. Sultansoy, Phys. Lett. B **443**, 359 (1998).
  - [19] M. Sahin, S. Sultansoy and S. Turkoz, Phys. Lett. B **689**, 172 (2010) [arXiv:1001.4505 [hep-ph]].
  - [20] A. N. Akay, H. Karadeniz, M. Sahin and S. Sultansoy, Europhys. Lett. **95**, 31001 (2011) [arXiv:1012.0189 [hep-ph]].
  - [21] J. Beringer *et al.* [Particle Data Group], Phys. Rev. D **86**, 010001 (2012).

- [22] F. Abe *et al.* [CDF Collaboration], Phys. Rev. Lett. **63**, 1447 (1989).
- [23] U. Baur and K. H. Streng, Phys. Lett. B **162**, 387 (1985).
- [24] W. Bartel *et al.*, Z Phys. C **36**, 15 (1987).
- [25] I. Abt *et al.* [H1 Collaboration], Nucl. Phys. B **396**, 3 (1993).
- [26] N. D. Christensen and C. Duhr, Comput. Phys. Commun. **180**, 1614 (2009) [arXiv:0806.4194 [hep-ph]].
- [27] C. Degrande, C. Duhr, B. Fuks, D. Grellscheid, O. Mattelaer and T. Reiter, Comput. Phys. Commun. **183**, 1201 (2012) [arXiv:1108.2040 [hep-ph]].
- [28] J. Alwall, M. Herquet, F. Maltoni, O. Mattelaer and T. Stelzer, JHEP **1106**, 128 (2011) [arXiv:1106.0522 [hep-ph]].
- [29] J. Pumplin, D. R. Stump, J. Huston, H. L. Lai, P. M. Nadolsky and W. K. Tung, JHEP **0207**, 012 (2002) [hep-ph/0201195].
- [30] J. Alwall, S. de Visscher and F. Maltoni, JHEP **0902**, 017 (2009) [arXiv:0810.5350 [hep-ph]].